



HAL
open science

Experimental and kinetic modeling study of n-pentane oxidation at 10 atm, Detection of complex low-temperature products by Q-Exactive Orbitrap

Nesrine Belhadj, Maxence Lailliau, Roland Benoit, Philippe Dagaut

► To cite this version:

Nesrine Belhadj, Maxence Lailliau, Roland Benoit, Philippe Dagaut. Experimental and kinetic modeling study of n-pentane oxidation at 10 atm, Detection of complex low-temperature products by Q-Exactive Orbitrap. *Combustion and Flame*, 2022, 235, pp.111723. 10.1016/j.combustflame.2021.111723 . hal-03500229

HAL Id: hal-03500229

<https://hal.science/hal-03500229>

Submitted on 22 Dec 2021

HAL is a multi-disciplinary open access archive for the deposit and dissemination of scientific research documents, whether they are published or not. The documents may come from teaching and research institutions in France or abroad, or from public or private research centers.

L'archive ouverte pluridisciplinaire **HAL**, est destinée au dépôt et à la diffusion de documents scientifiques de niveau recherche, publiés ou non, émanant des établissements d'enseignement et de recherche français ou étrangers, des laboratoires publics ou privés.

Copyright

Experimental and kinetic modeling study of n-pentane oxidation at 10 atm, Detection of complex low-temperature products by Q-Exactive Orbitrap

Nesrine Belhadj^{1,2}, Maxence Lailliau^{1,2}, Roland Benoit¹, Philippe Dagaut^{1,*}

¹ CNRS-INSIS, ICARE, 1C avenue de la Recherche Scientifique, 45071 Orléans cedex 2, France

² Université d'Orléans, rue de Chartres, 45100 Orléans, France

*Corresponding author:

Philippe Dagaut

CNRS-ICARE, Institut de Combustion, Aérothermique, Réactivité et Environnement

1C Avenue de la Recherche Scientifique

45071 Orléans Cedex 2, France

Tel: +33 (0)2 38 25 54 66

dagaut@cnrs-orleans.fr

ABSTRACT

Renewable feedstock such as biomass derivatives (hemicellulose, furfural) can be used to produce synthetic fuels, e.g., n-pentane, of interest for enhancing performance of diesel and gasoline engines. Whereas numerous studies of n-pentane have been published, its low temperature oxidation is not fully characterized and even recent kinetic models do not incorporate extended oxidation pathways which still need to be observed for n-pentane. In this context, a continuous flow fused-silica jet-stirred reactor (JSR) was used for studying the oxidation of 2500 ppm of n-pentane at 520–800 K, 10 atm (representative of piston engines operating conditions), an equivalence ratio of 0.5, and a residence time of 1.5 s. Oxidation products were analyzed in the gas phase using gas chromatography (thermal conductivity, TCD and flame ionization, FID), Fourier-transform infrared spectrometry (FTIR), and electron impact ionization-quadrupole mass spectrometry (EI-qMS). Gaseous products were also dissolved in acetonitrile for characterization using flow injection analysis (FIA), high-pressure and ultra-high-pressure liquid chromatography (HPLC and UHPLC) coupled to atmospheric pressure chemical ionization (APCI) and Q-Exactive[®]-Orbitrap high resolution mass spectrometry (HRMS). This allowed detecting lower and higher mass oxygenated molecules such as methyl vinyl ketone (MVK) and 2,5-dihydrofuran (C₄H₆O), 2-butanone (C₄H₈O), 3-pentene-2-one (C₅H₈O), pentanediones (C₅H₈O₂), cyclic ethers and pentanones (C₅H₁₀O), C₃–C₅ alkylhydroperoxides (C₃H₈O₂, C₄H₁₀O₂, C₅H₁₂O₂), C₂–C₅ alkenylhydroperoxides (C₂H₄O₂, C₃H₆O₂, C₄H₈O₂, C₅H₁₀O₂), C₃–C₅ keto-hydroperoxides (C₃H₆O₃, C₄H₈O₃, C₅H₁₀O₃), and highly oxygenated molecules (C₅H₈O₄, C₅H₁₂O₄, C₅H₁₀O₄, C₅H₁₀O₅, C₅H₁₀O₇) produced through multiply O₂ addition on fuel's radicals and internal H-shifts. Among these products 15 had not been reported before. Simulation of the present experiments showed discrepancies between experimental results and predictions.

Keywords: n-pentane, cool-flame, jet-stirred reactor, keto-hydroperoxides, Orbitrap, kinetic modeling

1. Introduction

Lignocellulosic biomass is a renewable feedstock used to produce alternative fuels. Furfural and hemicellulose can be used as precursors for the synthesis of n-pentane [1, 2] which has been proposed as a biofuel additive used to enhance performance of diesel and gasoline engines, as well as for its environmental benefits (reduction of NO_x, HC, and CO emissions) [3-5]. The low temperature oxidation of n-pentane has been studied for decades [6, 7]. More recently, Bugler et al. [8] carried out a theoretical study of pentane isomers oxidation. The formation of complex chemical combustion intermediates has been investigated by various modeling and experimental studies, using different techniques, e.g., rapid compression machine (RCM) and jet-stirred reactors (JSR) [9]. That experimental study of n-pentane oxidation using two JSR (81.2 and 39cm³, respectively) has been performed under the following experimental conditions: (i) JSR 1% of fuel at 1 atm, residence time of 2 s, and (ii) JSR 0.1% of fuel at 10 atm, residence time of 0.7 s. The temperature range studied was 500–1100 K, for equivalence ratio of 0.3-2. Two analytical methods were used: gas chromatography (TCD, FID, EI-MS) and Continuous Wave-Cavity Ring Down Spectroscopy (Cw-CRDS). Many oxygenated species (C₅ aldehydes, ketones, diones, etc.) have been detected. Rodriguez et al. [10] studied the low temperature oxidation of n-pentane in a jet-stirred reactor at atmospheric pressure and a residence time of 2 s. They investigated the formation of hydroperoxides (H₂O₂, C₁–C₂, and C₅ alkylhydroperoxides, alkenylhydroperoxides (C₃–C₅) and C₅ keto-hydroperoxides, by means of different types of mass spectrometry (i.e., synchrotron vacuum ultraviolet photoionization mass spectrometry (SVUV-PIMS) and single-photon-ionization mass spectrometry (SPI-MS) in addition to a spectroscopic method (Cw-CRDS). More recently, Bourgalais et al. [11] investigated the low-temperature oxidation of n-pentane using a JSR at atmospheric pressure, for a residence time of 3 s and two equivalence ratios (0.3 and 0.5). Alkenylhydroperoxides and other oxidized species could be characterized using i²PEPICO (double imaging PhotoElectron PhotoIon COincidence) spectroscopy.

Low-temperature oxidation intermediates are formed by combustion reactions requiring oxygen addition onto fuel's radicals followed by different chemical reactions such as isomerization, intramolecular rearrangement and molecular decomposition. As observed previously for heavier hydrocarbons and oxygenates (esters, aldehydes, alcohols, ethers), oxidation can proceed much further than previously reported in combustion studies [12-23]. In our recent combustion works, we could observe the formation of highly oxygenated molecules (HOMs) resulting from more than two oxygen additions on fuels' radicals [17-23]. Interestingly, HOMs produced through multiple O₂ addition on fuel's radicals and internal H-shifts, are considered important chemicals in atmospheric chemistry, especially for the evolution and growth of secondary organic aerosols (SOA) [24-26]. Indeed, similarities between low-temperature combustion products and tropospheric oxidation products have been reported in a recent study of the oxidation of limonene in a JSR and data taken from the literature [27].

The aim of this study is twofold: (i) further investigate experimentally the formation of low temperature oxidation products of n-pentane by developing and utilizing separation techniques coupled to high resolution mass spectrometry to confirm extended oxidation processes observed for larger hydrocarbons and oxygenates (Supplementary Material, Scheme 1) and (ii) verify the predictive capabilities of recent kinetic models. To this end, we oxidized 2500 ppm of n-pentane reacting in a JSR at a pressure of 10 atm (Section 2). As described in the Experimental Section, several analytical techniques were used to identify oxygenated intermediates such as cyclic ethers, diones, alkylhydroperoxides, alkenylhydroperoxides, keto-hydroperoxides, and highly oxygenated molecules (HOMs). They included gas chromatography (GC), Fourier Transform Infrared spectrometry (FTIR), liquid chromatography (HPLC, UHPLC), and high-resolution mass spectrometry (Orbitrap Q-Exactive). Quantitative measurements were made by GC (FID, TCD) and FTIR. Experimental results are compared to simulations using a previously published reaction mechanism which includes third-O₂ addition on fuel's radicals. Formation pathways of several low temperature intermediates are presented.

2. Experimental methods

2.1 JSR experiments

The oxidation of n-pentane at low temperature was performed in a JSR described previously [28, 29] (see refs [28, 30] for a schematic representation of the experimental setup). This experimental setup has been used in previous works concerning the kinetics of oxidation of gas and liquid fuels, e.g., [31-33]. The JSR is located inside a temperature-controlled oven (~ 1.5 kW), which is surrounded by insulating ceramic wool and a pressure-resistant stainless-steel housing, allowing the reactor to be maintained at a desired working temperature and pressure. n-Pentane (>99% pure from Sigma Aldrich) was vaporized and atomized using an in-house setup [33]. The fuel-N₂ and O₂-N₂ mixtures flowed separately to the four JSR injectors (nozzles of 1 mm I.D.) to avoid premature fuel oxidation. N₂ and O₂ flow rates were controlled by mass flow meters (Brooks). The fuel was pumped using an HPLC pump (Shimadzu LC10 AD VP) equipped with an online degasser (Shimadzu DGU-20 A3). The experimental conditions are listed in Table 1. Thermal homogeneity on the vertical axis of the reactor was checked using a Pt-Pt/Rh-10% thermocouple (wires of 100 μm insulated inside a thin wall fused-silica housing). Gradients of < 1 K/cm were measured. The gaseous oxidation samples were introduced into Pyrex bulbs for GC analysis. However, FIA and LC-HRMS analyses require liquid samples. Thus, gas samples exiting the sonic probe were directed to an amber glass vial filled with acetonitrile for 75 min (0°C, 25 mL). The vial was located in a container filled with water-melting ice. In order to limit thermal degradation, oxidation samples were stored at -15°C in a freezer for future chemical analyses. We noticed no significant degradation of relatively unstable products (e.g., ketohydroperoxides, hydroperoxides, HOMs) for the 6 first months of storage.

Table1. JSR experimental conditions.

Initial n-pentane, O ₂ , and N ₂ mole fractions	0.25 %, 4 %, 95.75 %
Equivalence ratio (ϕ)	0.5
Residence time (s)	1.5
Pressure (atm)	10
Temperature range (K)	520 to 800

2.2 Analytical methods

Different complementary chromatographic procedures and techniques (GC, HPLC, UHPLC) were developed and used to analyze samples of n-pentane oxidation (see Supplementary Materials, Table S1 for conditions). Gas chromatography was used to analyze light chemicals. A TCD was used to measure H₂ and O₂. FID was used to measure hydrocarbons, aldehydes, ketones, diones, ethers, and alcohols. Formaldehyde, carboxylic acids, CO, CO₂ and H₂O were quantified using an FTIR. To quantify reactants and products, detectors were calibrated using standards. For products which could not be calibrated, we used the effective carbon number method. Overall uncertainties were estimated of the order of 15%.

Flow injection analysis (FIA) using a syringe pump was also used to provide a global compound signal with no chromatographic separation. Only the FIA, HPLC and UHPLC analyses were coupled to a Thermo Scientific™ Orbitrap® Q-Exactive high resolution mass spectrometer (maximum resolution $m/\Delta m = 140,000$ at m/z 200, mass accuracy <1 ppm RMS, and $m/z \geq 50$). HPLC and UHPLC were used for separating products, and particularly isomers having the same exact mass determined by HRMS and different polarities. Soft ionization by atmospheric pressure chemical ionization (APCI) was employed to produce ions in positive (M+H)⁺ and negative (M-H)⁻ modes (see Supplementary Materials, Table S2 for ionization settings). In order to increase sensitivity during HPLC and UHPLC analyses, the targeted Selected Ion Monitoring acquisition mode (t-SIM) was used to collect a narrow mass range. MS/MS (tandem mass spectrometry) analyses were conducted at a higher energy collisional dissociation (HCD) of 10 eV.

As in our previous works [17-22, 27], several analytical chemical procedures were applied to improve the detection of species or to reveal specific functional groups. For example, 2,4-dinitrophenylhydrazine (2,4-DNPH) was used to derive the carbonyl function of aldehydes and ketones formed during n-pentane oxidation. This practice is particularly interesting for aldehydes with $m/z < 50$ which cannot be detected by Orbitrap Q-Exactive. Moreover, this method allows to confirm the presence of the carbonyl function in other oxidized compounds such as ketohydroperoxides (KHPs). The derivatization procedure was as follows: 20 μ L of a diluted H₃PO₄ solution (50 μ L of acid in 1 mL of

ACN) and 100 μL of a saturated solution of 2,4-DNPH (2 g in 100 ml of ACN) were added to 1 ml of a n-pentane oxidation sample (600 K). Negative APCI mode was used to ionize DNPHhydrazone derivatives. Deuterium oxide (D_2O) was used to conduct hydrogen/deuterium (H/D) exchange and confirm the presence of the hydroperoxy (OOH) function in hydroperoxides, ketohydroperoxides, and HOMs. To this end, 150 μL of D_2O were added to 500 μL of n-pentane oxidation sample; the sample reacted at room temperature for 20 min. Analyses were performed in FIA APCI (+/-) modes (Supplementary Materials, Table S2.).

3. Modeling

Kinetic modeling using the PSR (perfectly stirred reactor) computer code [34] from the Chemkin II package [35] was carried out. Third O_2 addition reactions were presented in a recent kinetic reaction mechanism [15] proposed by Wang and Sarathy (WS model). Low- and high-temperature chemistry are included in that scheme which involves 1188 species and 4959 reactions. The computations showed that in the low-temperature oxidation region, n-pentane is mainly consumed through H-atom abstraction by OH radicals produced by the decomposition of ketohydroperoxides. A shift in temperature between the present modeling and experimental data was observed for all concentration profiles, as already noticed for the oxidation of n-hexane under similar conditions, also using the WS model [23].

4. Results and discussion

n-Pentane oxidation was conducted in a JSR at 10 atm (Table 1). Using FTIR, GC (FID, TCD, EI-qMS) and LC (APCI-HRMS) analytical techniques (Supplementary Materials, Table S1) we could identify and/or obtain mole fraction profiles of several intermediate species and products formed during n-pentane oxidation.

The high-resolution mass spectrometer (Orbitrap Q-Exactive) used here has a wide mass range. However, it is characterized by a minimum scan range m/z of 50 which precludes analyzing low mass species such as: CH_4 (MW = 16), C_2H_4 (MW = 28), CH_2O (MW = 30), CH_4O (MW = 32), C_3H_6 (MW = 42), $\text{C}_2\text{H}_4\text{O}$ (MW = 44), CH_2O_2 (MW = 46) and $\text{C}_3\text{H}_4\text{O}$ (MW = 56). As indicated previously in the experimental procedure, a DNPH derivatization was used to characterize carbonyls with mass <50 in samples, i.e., for formaldehyde (CH_2O), acetaldehyde ($\text{C}_2\text{H}_4\text{O}$) and acrolein ($\text{C}_3\text{H}_4\text{O}$) (Supplementary Materials, Table S3). Unfortunately, other molecules ($m/z \geq 50$) like 1,3-pentadiene and 1,3-butadiene could not be characterized by HRMS due to the unavailability of standards. Therefore, these species were identified by other analytical techniques such as FTIR and GC (Supplementary Materials, Table S1). Their mole fraction profiles were plotted and compared to modeling results obtained using the WS model [15]. Figures 1 and 2 show some examples of chemical species not detected by HRMS. One can see a similar reactivity between experimental (GC, FTIR) and modeling profiles of some compounds such as n-pentane, O_2 , CO, CH_4 , CH_2O . However, discrepancies between experimental data and simulations appeared for several chemical intermediates. For example, we noticed an under-prediction of methanol, ethanol, and 1,3-pentadiene, which could be explained by the absence of some reaction

pathways in the kinetic model (their formation pathways included in the model are detailed in Supplementary Materials, Scheme S2). The over-prediction of formic acid and butanal could be due to the use of inappropriate kinetics in the model (see Supplementary Materials, Scheme S2 for formation pathways). In the present conditions, at 600 K, the oxidation of formaldehyde by OH gives 68% of formic acid, and 32% are produced by the $\text{CH}_3\text{CO} + \text{OH}$ reaction which is not present in the NIST kinetic database. One can estimate, the kinetics of these reactions are causing the observed over-prediction of formic acid.

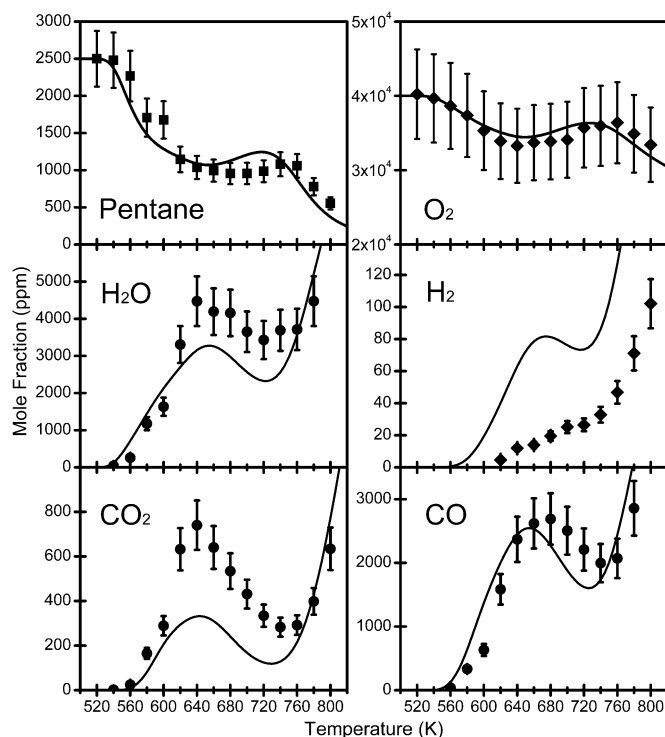


Fig. 1. Evaluation of Fuel, O_2 , CO_2 , CO , H_2O and H_2 mole fraction profiles obtained during oxidation of 2500 ppm of n-pentane in JSR at a pressure of 10 atm, $\phi = 0.5$ and residence time of 1.5 s. Experimental results (symbols) using GC-FID (n-pentane), GC-TCD (O_2 and H_2) and FTIR (CO_2 , CO , H_2O) are compared to simulations (lines) using the WS model.

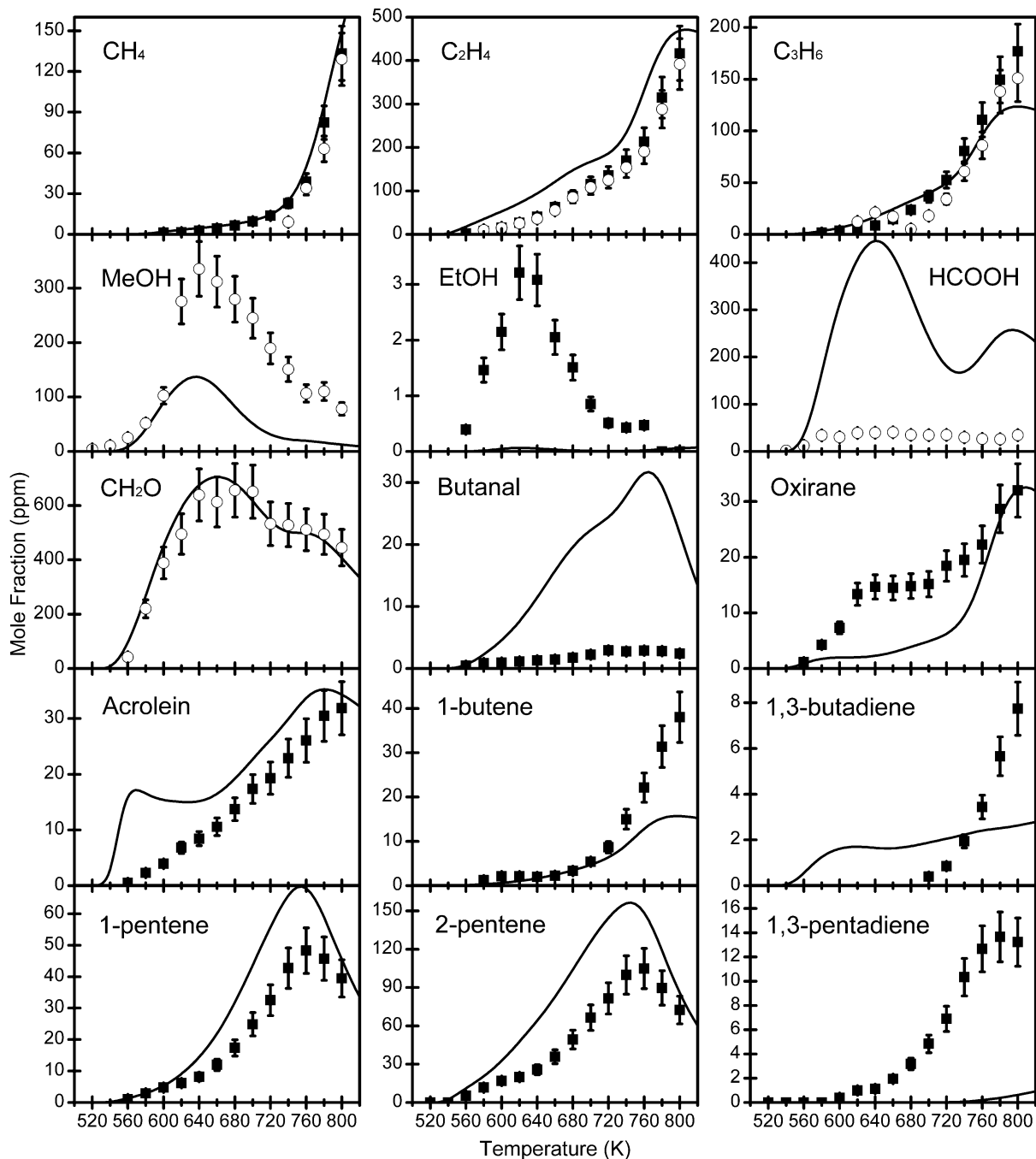


Fig. 2. Comparison between experimental mole fraction of organic species and simulations (using the WS model) for the oxidation of 2500 ppm of n-pentane in JSR at a pressure of 10 atm, ($\phi = 0.5$, residence time of 1.5 s). Symbols: data obtained by GC-FID (square) and FTIR (circle).

Some compounds could be characterized by at least two of the different analytical methods (HPLC, GC, and FTIR) (Supplementary Materials, Table S1), for example, C_4H_6O corresponding to methyl vinyl ketone (MVK) and 2,5-dihydrofuran (2,5-DHF), C_4H_8O corresponding to 2-butanone, and $C_2H_4O_2$ which corresponds to acetic acid. Their mole fraction profiles were plotted in Figure 3. The WS kinetic model underestimates the formation of acetic acid and 2,5-DHF (very low mole fraction), which could indicate that they are formed by other reaction pathways than those included in the kinetic model

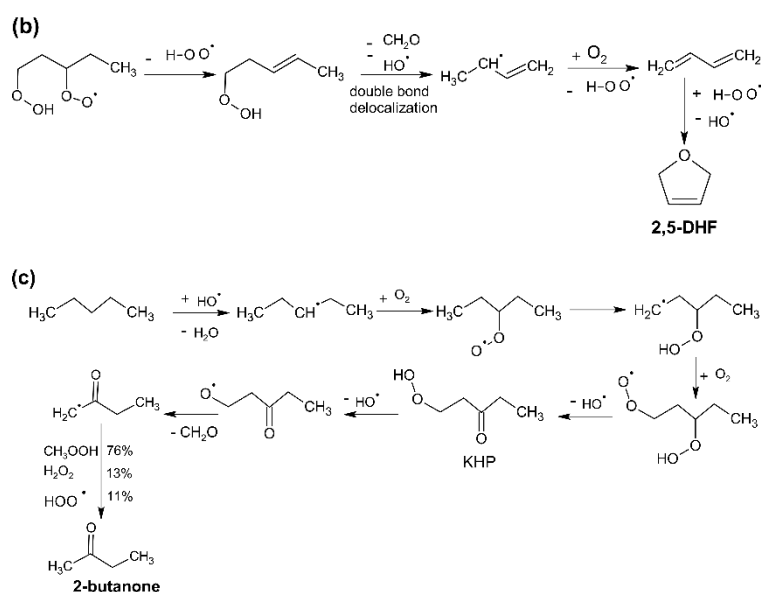


Fig. 4. Formation pathways for MVK (a), 2,5-DHF (b), and 2-butanone (c) from kinetic modeling at 600 K.

Due to its high resolution, the Orbitrap Q-Exactive mass spectrometer, coupled to liquid phase analytical methods (FIA, HPLC and UHPLC), allows the detection of a wide range of compounds with high mass accuracy (m/z 50-200 presently). Organic compounds were classified according to their chemical formula, i.e. $C_5H_{12}O_x$ ($x=2-6$), $C_5H_{10}O_x$ ($x=1-7$), $C_5H_8O_x$ ($x=1-7$), $C_5H_6O_x$ ($x=1-6$), $C_5H_4O_x$ ($x=1-5$), C_nH_{2n} ($n=4,5$), C_nH_{2n-2} ($n=4,5$), $C_nH_{2n}O$ ($n=3-5$), $C_nH_{2n-2}O$ ($n=3-5$), $C_nH_{2n-4}O$ ($n=3-4$), $C_nH_{2n+2}O_2$ ($n=5$), $C_nH_{2n}O_2$ ($n=2-5$), $C_nH_{2n-2}O_2$ ($n=3-5$), $C_nH_{2n-4}O_2$ ($n=3-5$), and $C_nH_{2n}O_3$ ($n=1-5$). Aldehydes, ketones, carboxylic acids and diones produced during n-pentane low-temperature oxidation, were identified by analyzing standards on a C_{18} UHPLC column and APCI (+/-) (Supplementary Material, Table S4). Other important low temperature oxidation oxygenated species are presented in Table 2.

Table 2. Products of n-pentane oxidation in a JSR at 600 K and 10 atm. H/D exchange was performed (see Section 3.2) before FIA.

M (g/mole)	Compounds		Ionization mode			
			APCI (+)		APCI (-)	
	Formula	Name	m/z [M+H] ⁺	Signal (a.u)	m/z [M-H] ⁻	Signal (a.u)
60	$C_2H_4O_2$	Ethenyl-hydroperoxide*, acetic acid	61.0283	1.9E6	59.0139	2.1E7
61	$C_2H_3D_1O_2$	Ethenyl-hydroperoxide-d ₁ *, acetic acid-d ₁	62.0346	2.1E6	60.0201	9.9E6
62	$C_2H_6O_2$	Ethyl hydroperoxides	-	§	-	§
74	$C_2H_2O_3$	Unsaturated C ₂ -KHP*	-	-	72.9931	3.9E6
75	$C_2H_1D_1O_3$	Unsaturated C ₂ -KHP-d ₁ *	-	-	73.9994	3.6E5

74	C ₃ H ₆ O ₂	Propenyl (Allyl)-hydroperoxides and propanoic acid	75.0438	1.4E6	73.0295	3.4E6
75	C ₃ H ₅ D ₁ O ₂	Propenyl (Allyl)-hydroperoxides-d ₁ , propanoic acid-d ₁	76.0501	1.0E6	74.0358	7.0E5
76	C ₂ H ₄ O ₃	C ₂ -KHP*	77.0231	7.2E3	75.0088	2.9E7
77	C ₂ H ₃ D ₁ O ₃	C ₂ -KHP-d ₁ *	-	§	76.0151	1.2E7
76	C ₃ H ₈ O ₂	Propyl-hydroperoxide*	77.0594	1.6E4	-	§
77	C ₃ H ₇ D ₁ O ₂	Propyl-hydroperoxide-d ₁ *	78.0658	4.5E3	-	§
86	C ₅ H ₁₀ O	Cyclic ethers, pentanones and Valeraldehyde	87.0802	2.1E7	85.0658	4.4E2
87	C ₅ H ₉ D ₁ O	Valeraldehyde-d ₁	88.0864	1.1E7	-	§
88	C ₄ H ₈ O ₂	Butenyl-hydroperoxides and butyric acid	89.0594	3.2E6	87.0452	1.8E6
89	C ₄ H ₇ D ₁ O ₂	Butenyl-hydroperoxides and butyric acid-d ₁	90.0656	2.3E6	88.0515	3.3E6
88	C ₃ H ₄ O ₃	Unsaturated C ₃ -KHP*	-	-	87.0088	3.6E7
89	C ₃ H ₃ D ₁ O ₃	Unsaturated C ₃ -KHP-d ₁ *	-	-	88.0151	1.4E7
90	C ₄ H ₁₀ O ₂	Butyl-hydroperoxides*	91.0750	6.5E4	-	§
91	C ₄ H ₉ D ₁ O ₂	Butyl-hydroperoxides-d ₁ *	92.0814	4.1E4	-	§
90	C ₃ H ₆ O ₃	C ₃ -KHP*	91.0386	1.2E5	89.0245	3.4E7
91	C ₃ H ₅ D ₁ O ₃	C ₃ -KHP-d ₁ *	92.0451	1.3E5	90.0307	5.0E7
100	C ₅ H ₈ O ₂	Diones, 2-Me-THF-3-one and 3-tetrahydropyranone	101.0593	1.1E8	99.0452	1.4E7
102	C ₅ H ₁₀ O ₂	Pentenyl-hydroperoxides, and valeric acid	103.0750	6.3E7	101.0608	3.5E4
103	C ₅ H ₉ D ₁ O ₂	Pentenyl-hydroperoxides-d ₁ , valeric acid-d ₁	104.0814	9.4E7	102.0671	9.4E4
102	C ₄ H ₆ O ₃	Unsaturated C ₄ -KHP*	103.0386	6.8E4	101.0244	6.6E6
103	C ₄ H ₅ D ₁ O ₃	Unsaturated C ₄ -KHP-d ₁ *	104.0449	1.9E4	102.0307	6.9E6
104	C ₅ H ₁₂ O ₂	pentyl hydroperoxides	105.0906	3.5E5	-	§
105	C ₅ H ₁₁ D ₁ O ₂	pentyl hydroperoxides-d ₁ *	106.0970	9.1E5	-	-
104	C ₄ H ₈ O ₃	C ₄ -KHP*	105.0543	1.9E5	103.0401	1.2E7
105	C ₄ H ₇ D ₁ O ₃	C ₄ -KHP-d ₁ *	106.0605	1.7E5	104.0464	3.3E7
116	C ₅ H ₈ O ₃	unsaturated C ₅ -KHP *	117.0542	1.2E6	115.0401	3.7E7
117	C ₅ H ₇ D ₁ O ₃	unsaturated C ₅ -KHP-d ₁ *	118.0605	1.1E6	116.0464	4.4E7
118	C ₅ H ₁₀ O ₃	C ₅ -KHP	119.0702	6.1E6	117.0556	6.3E7
119	C ₅ H ₉ D ₁ O ₃	C ₅ -KHP-d ₁	120.0761	5.7E6	118.0620	2.0E8

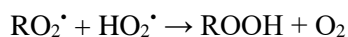
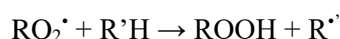
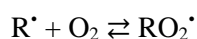
132	C ₅ H ₈ O ₄	Diketo-hydroperoxides*	133.0491	8.0E3	131.0350	6.1E7
133	C ₅ H ₇ D ₁ O ₄	Diketo-hydroperoxides-d ₁ *	134.0554	5.6E3	132.0412	4.3E6
134	C ₅ H ₁₀ O ₄	C ₅ - unsaturated dihydroperoxides*	135.0648	1.1E4	133.0504	2.0E4
135	C ₅ H ₉ D ₁ O ₄	C ₅ - unsaturated dihydroperoxides-d ₁ *	136.0710	8.9E3	134.0569	2.3E5
136	C ₅ H ₈ D ₂ O ₄	C ₅ - unsaturated dihydroperoxides-d ₂ *	-	§	135.0632	1.9E5
136	C ₅ H ₁₂ O ₄	C ₅ -dihydroperoxides*	137.0808	§	135.0658	4.7E2
137	C ₅ H ₁₁ D ₁ O ₄	C ₅ -dihydroperoxides-d ₁ *	138.0875	2.9E3	136.0720	2.6E2
138	C ₅ H ₁₀ D ₂ O ₄	C ₅ -dihydroperoxides-d ₂ *	139.0933	§	137.0787	§
150	C ₅ H ₁₀ O ₅	Keto dihydroperoxides*	-	-	149.0455	1.6E5
151	C ₅ H ₉ D ₁ O ₅	Keto dihydroperoxides-d ₁ *	-	-	150.0518	1.2E6
152	C ₅ H ₈ D ₂ O ₅	Keto dihydroperoxides-d ₂ *	-	-	151.0581	1.8E6
182	C ₅ H ₁₀ O ₇	Keto trihydroperoxides*	-	-	181.0356	4.5E2
183	C ₅ H ₉ D ₁ O ₇	Keto trihydroperoxides-d ₁ *	-	-	182.0417	7.2E4
184	C ₅ H ₈ D ₂ O ₇	Keto trihydroperoxides-d ₂ *	-	-	183.0479	1.8E5
185	C ₅ H ₇ D ₃ O ₇	Keto trihydroperoxides-d ₃ *	-	-	-	§

Note: - not detected, §: below detection limit, *: not reported before.

Some specific low-temperature oxygenated molecules have attracted our attention, their HRMS analyses are detailed hereafter.

4.1 Hydroperoxides: C₃H₈O₂, C₄H₁₀O₂ and C₅H₁₂O₂

The peroxidation of fuel's radicals and H-atom abstraction by RO₂' can yield hydroperoxides:



Thanks to use of high-resolution mass spectrometry, signals corresponding to propyl, butyl, and pentyl hydroperoxides (C₃H₈O₂, C₄H₁₀O₂, C₅H₁₂O₂) were detected using FIA coupled to positive APCI and HRMS (C₃H₉O₂⁺, *m/z* 77.0594, C₄H₁₁O₂⁺, *m/z* 91.0750, C₅H₁₃O₂⁺, *m/z* 105.0906). Their profiles were plotted and compared (Fig. 5). Only the simulated profile of C₅H₁₂O₂ could be presented because the two other alkyl hydroperoxides are not present in the WS model.

We can see from Figure 5 that the three hydroperoxides are not formed at the same level (C₅ > C₃ > C₄) and do not peak at the same temperature (600 K for C₅H₁₂O₂, 580 K for C₃H₈O₂ and 620 K for C₄H₁₀O₂). Due to their weak intensities, UHPLC analyses of C₃ and C₄ hydroperoxides did not lead to useful

chromatograms. Only UHPLC analyses of $C_5H_{12}O_2$ generated a low chromatographic signal in the range of 10^4 , which is close to the detection limit of our HRMS instrument.

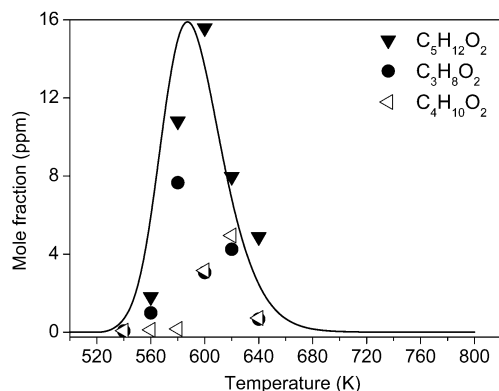


Fig. 5. Evolution of $C_3H_9O_2^+$ (m/z 77.0594), $C_4H_{11}O_2^+$ (m/z 91.0750) and $C_5H_{13}O_2^+$ (m/z 105.0906) profiles corresponding to alkyl hydroperoxides $C_3H_8O_2$, $C_4H_{10}O_2$ and $C_5H_{12}O_2$ formed during the oxidation of n-pentane in JSR at 10 atm. Experimental results were obtained using FIA-positive APCI HRMS. The line represents the simulated $C_5H_{12}O_2$ mole fraction. HRMS results were scaled to computations. Experimental errors are estimated to be $\sim 40\%$.

4.2 Alkenylhydroperoxides: $C_2H_4O_2$, $C_3H_6O_2$, $C_4H_8O_2$, and $C_5H_{10}O_2$

Hydroperoxides isomers corresponding to $C_5H_{12}O_2$ can undergo H-atom abstraction followed by O_2 addition and intramolecular rearrangement to form pentenyl hydroperoxides ($C_5H_{10}O_2$) and lower mass alkenyl hydroperoxides including $C_2H_4O_2$, $C_3H_6O_2$ and $C_4H_8O_2$. Proposed formation pathways for C_2 , C_3 , C_4 , and C_5 alkenyl hydroperoxides in the WS model are illustrated in Figure 6.

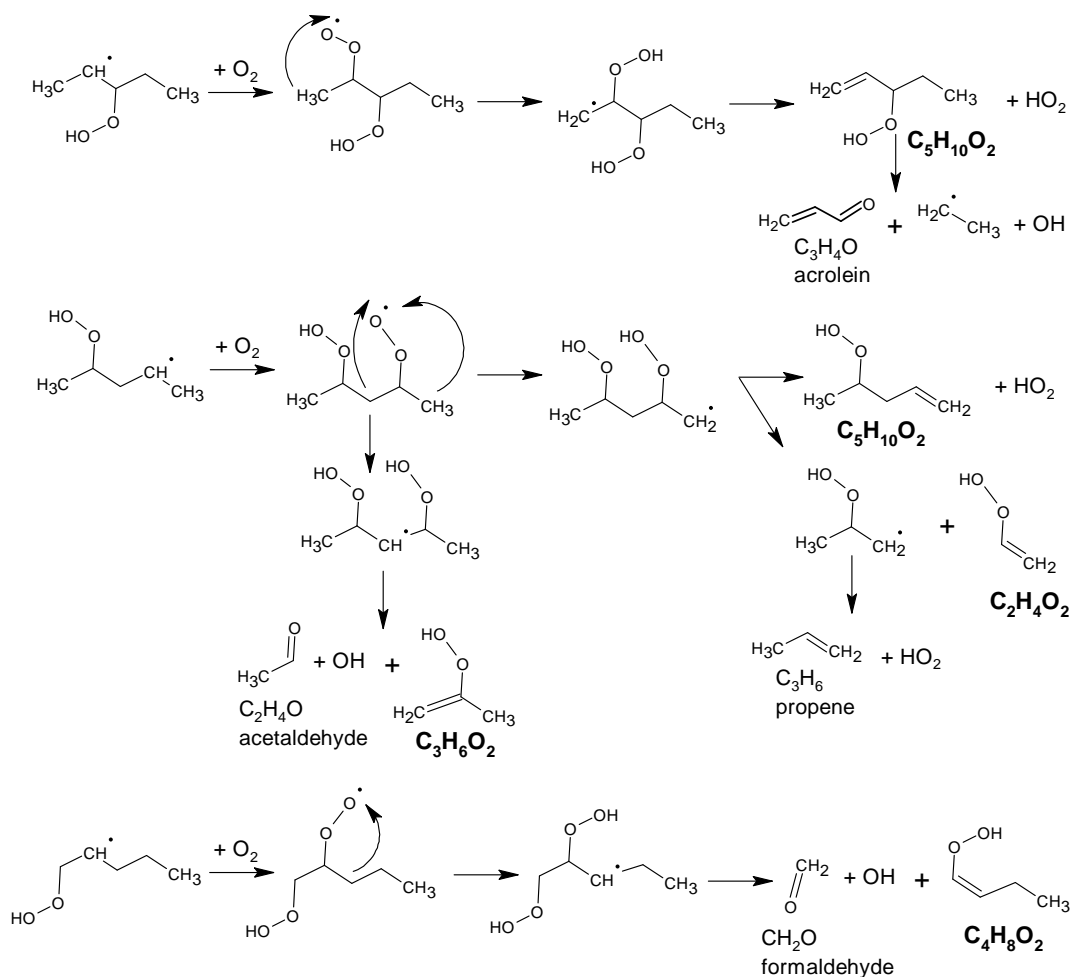


Fig. 6. Simulated formation pathways of ethenyl, propenyl, butenyl, and pentenyl hydroperoxides ($C_2H_4O_2$, $C_3H_6O_2$, $C_4H_8O_2$ and $C_5H_{10}O_2$) during the low temperature oxidation of n-pentane.

FIA signals corresponding to $C_2H_4O_2$, $C_3H_6O_2$, $C_4H_8O_2$, and $C_5H_{10}O_2$ species were detected in both positive APCI ($C_2H_5O_2^+$ at m/z 61.0283), $C_3H_7O_2^+$ at m/z 75.0438, $C_4H_9O_2^+$ at m/z 89.0594, and $C_5H_{11}O_2^+$ at m/z 103.0750 and negative APCI ($C_2H_3O_2^-$ at m/z 59.0139, $C_3H_5O_2^-$ at m/z 73.0295, $C_4H_7O_2^-$ at m/z 87.0542, and $C_5H_9O_2^-$ at m/z 101.0608), see Table 2. We could note that $C_5H_{10}O_2$ isomers are better ionized in positive APCI (signal $\sim 10^7$) than in negative mode (signal $\sim 10^4$), unlike $C_2H_4O_2$, $C_3H_6O_2$, and $C_4H_8O_2$. That can be explained by a better ionization of these C_2 , C_3 and C_4 alkenyl hydroperoxides in negative APCI or by the presence of the corresponding carboxylic acids (acetic, propanoic, and butyric acid) for which the existence of acid-labile hydrogen favors a deprotonation, generating a stronger signal in negative mode. This comparison may indicate the presence of valeric acid in n-pentane oxidation samples. As indicated previously, acetic acid and propanoic acid are potentially produced through the Korcek mechanism [36] (Supplementary Materials, Fig. S1).

Reversed-phase UHPLC coupled to positive and negative APCI showed the presence of several chromatographic peaks for $C_2H_4O_2$, $C_3H_6O_2$, $C_4H_8O_2$, and $C_5H_{10}O_2$ (Fig. 7), which implies the presence of several isomers of these alkenylhydroperoxides. The chromatogram of $C_2H_4O_2$ obtained in negative

APCI shows the presence of acetic acid at a retention time of 1.56 min in addition to other peaks which may be attributed to ethenyl hydroperoxides. Analysis of $C_3H_6O_2$ reveals co-elution between propanoic acid (Rt 2.98 min) and another compound (Rt 2.62 min) which could be a propenyl hydroperoxide. Thus, the recorded $C_3H_6O_2$ profile can be somewhat biased. $C_4H_8O_2$ analyses showed the presence of several co-eluted products; butyric acid was identified at 5.35 min (weak signal). A valeric acid standard was also analyzed; the comparison of its retention time (10.08 min) with the chromatographic peaks obtained after APCI(+/-) HRMS analyses of $C_5H_{10}O_2$ reveals the absence of valeric acid in the oxidized n-pentane sample (Fig. 7), which confirms the hypothesis put forward after the FIA analysis.

Figure 8 presents signals attributed to C_2 , C_3 , C_4 , and C_5 alkenylhydroperoxides. One can observe that the formation of butenyl hydroperoxides $C_4H_8O_2$ is low compared to that of $C_2H_4O_2$, $C_3H_6O_2$, and $C_5H_{10}O_2$. This can be explained by the fact it is formed via a minor C_5 hydroperoxy radical (Fig. 6).

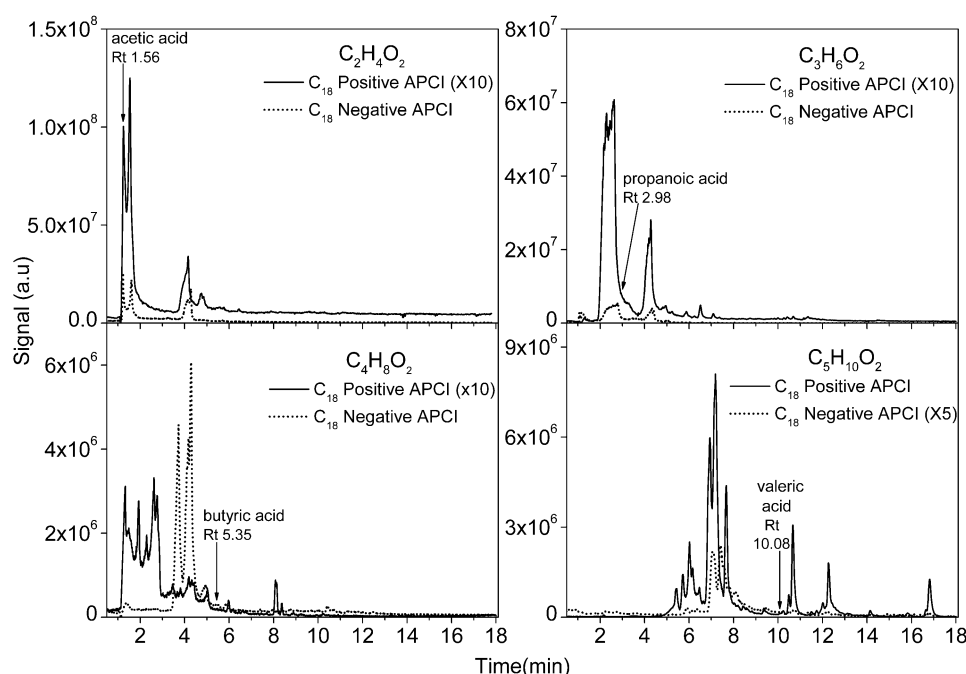


Fig. 7. Chromatograms showing the formation of C_2 , C_3 , C_4 and C_5 alkenylhydroperoxides. The analyses were performed using a C_{18} UHPLC coupled to APCI(+)-HRMS ($C_2H_5O_2^+$ at m/z 61.0283, $C_3H_7O_2^+$ at m/z 75.0438, $C_4H_9O_2^+$ at m/z 89.0594, and $C_5H_{11}O_2^+$ at m/z 103.0750), and APCI(-)-HRMS ($C_2H_3O_2^-$ at m/z 59.0139, $C_3H_5O_2^-$ at m/z 73.0295, $C_4H_7O_2^-$ at m/z 87.0452, and $C_5H_9O_2^-$ at m/z 101.0608). Retention times in min were: acetic acid Rt= 1.56 min, propanoic acid Rt= 2.98 min, butyric acid Rt= 5.35 min, and valeric acid Rt= 10.08 min.

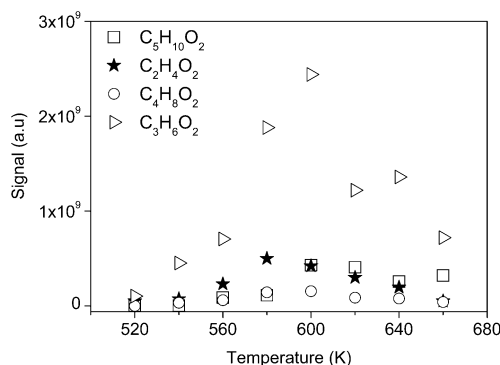
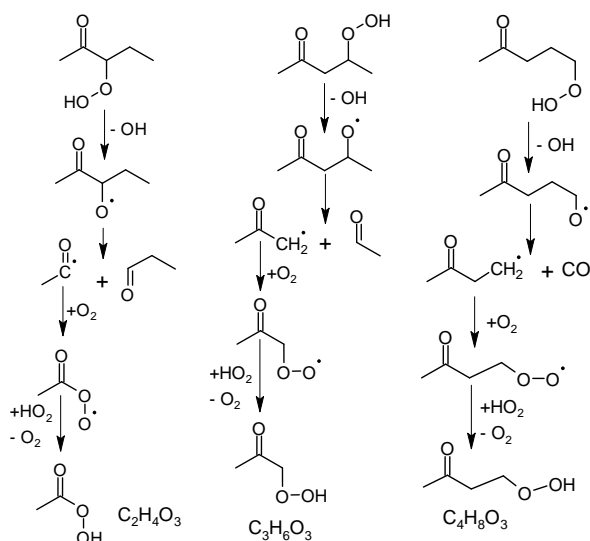


Fig. 8. Comparison between C₂, C₃, C₄ and C₅ alkenyl hydroperoxides formed during the low temperature oxidation of n-pentane. C₂, C₃ and C₄ alkenyl hydroperoxides profiles were obtained using C₁₈ UHPLC APCI(-)-HRMS (*m/z* 59.0139, 73.0295, and 87.0452 respectively). The C₅ profile was acquired by UHPLC APCI(+)-HRMS (*m/z* 103.0750). Experimental errors are estimated to be ~ 40%.

4.3 Ketohydroperoxides: C₂H₄O₃, C₃H₆O₃, C₄H₈O₃ and C₅H₁₀O₃

Ketohydroperoxides are characteristic chemical species of fuel's low-temperature oxidation. Besides the main autoxidation pathway in combustion, producing KHPs, i.e., Fuel + X[•] (OH[•], H[•], O[•], HO₂[•], O₂ etc.) → R[•] + XH; R[•] + O₂ → RO₂[•] → [•]QOOH (H-shift); [•]QOOH + O₂ → [•]OOQOOH → HOOQ[•]=O + [•]OH, other neglected oxidation mechanisms may play a role in combustion, i.e., 2 RO₂[•] → ROOOOR → 2 RO[•] + O₂; RO[•] → [•]QOH (H-shift); [•]QOH + O₂ → [•]OOQOH → OQ[•]OH + [•]OH. HRMS analyses allowed us to characterize signals relating to various chemical species having the same exact mass as C₂-C₅ ketohydroperoxides, i.e. C₂H₄O₃, C₃H₆O₃, C₄H₈O₃ and C₅H₁₀O₃. Scheme 1 shows the reaction scheme leading to the formation of C₂, C₃, and C₄ KHPs in the WS model.



Scheme 1. Formation of C₂H₄O₃, C₃H₆O₃, and C₄H₈O₃ KHPs in the WS model.

FIA-APCI analyses in positive and negative modes revealed the presence of C₃, C₄, and C₅ KHPs (Table 2). DNPH derivatization indicated the presence of DNPHhydrazone derivatives for C₂, C₃, C₄, and

C₅ KHPs (C₃H₈O₆N₄, C₉H₁₀O₆N₄, C₁₀H₁₂O₆N₄, and C₁₁H₁₄O₆N₄ respectively) (Supplementary Materials, Table S3), which confirms the presence of a carbonyl function in C₃H₆O₃, C₄H₈O₃, and C₅H₁₀O₃ species. Thanks to the use of a Silica Ascentis HPLC column, chromatographic signals corresponding to C₃H₆O₃ and C₄H₈O₃ using APCI(–)-HRMS (C₃H₅O₃[–] at *m/z* 89.0245 and C₄H₇O₃[–] at *m/z* 103.0401) were detected.

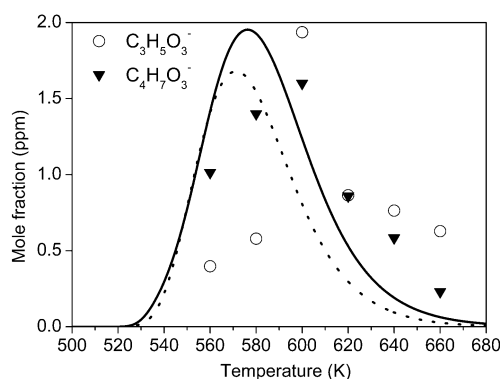


Fig. 9. Evolution of C₃H₅O₃[–] (*m/z* 89.0245), C₄H₇O₃[–] (*m/z* 103.0401) profiles corresponding to ketohydroperoxides C₃H₆O₃, and C₄H₈O₃ formed during the oxidation of n-pentane in JSR at 10 atm. Experimental data (Symbols) were scaled to modeling results (continuous line for C₃H₆O₃ and dotted line for C₄H₈O₃). Experimental results were obtained using a Silica HPLC column and APCI(–)-HRMS. HRMS errors are estimated to be ~ 40%.

The analysis of C₅H₁₀O₃ isomers was first performed on a C₁₈ UHPLC column. Unfortunately, this chromatographic column does not seem to be adequate for separating C₅H₁₀O₃ isomers. Thus, a Silica HPLC column was tested (chromatographic settings are given in Supplementary Materials, Table S1). Silica HPLC analyses showed the presence of several chromatographic peaks corresponding to C₅H₁₀O₃ isomers in both positive (C₅H₁₁O₃⁺ at *m/z* 119.0702) and negative (C₅H₉O₃[–] at *m/z* 117.0556) APCI modes (Fig. 10a). The comparison between chromatograms obtained with these two ionization modes confirms that negative APCI gives a better signal than positive APCI (Table 2 and Fig. 10a). In order to calculate peaks areas and plotting their profiles as a function of JSR temperature, a Gaussian curve fitting algorithm, with a fixed width at half maximum peak intensity, was applied to determine the different contributions of C₅H₁₀O₃ isomers observed in positive (C₅H₁₁O₃⁺, *m/z* 119.0702) and negative (C₅H₉O₃[–], *m/z* 117.0556) APCI modes (Supplementary Materials, Fig. S2 a and b). Then, the data were compared to simulated C₅H₁₀O₃ KHPs profiles, and allowed identifying potential KHPs having the same behavior as predicted by the WS kinetic model. Profiles that significantly differ from the model were considered to correspond to other C₅H₁₀O₃ species.

The chromatograms obtained using positive ionization revealed at least nine contributions of C₅H₁₁O₃⁺ species (Supplementary Materials, Fig. S2a). However, none of them corresponds to the predicted profile of KHPs as a function of temperature. This can be explained by co-elution of KHPs with other chemical species having the same molecular formula. We can notice that the positive

ionization reveals the presence of a chromatographic peak which is absent in chromatograms obtained in negative APCI (Rt 4 min), Fig. 10a. This implies that this chromatographic peak should correspond to a compound having the same mass as $C_5H_{10}O_3$ KHPs but not ionizable in negative mode, i.e., without deprotonation sites to form $[M-H]^-$. LC analyses using negative mode APCI revealed the presence of five chromatographic peaks (Supplementary Materials, Fig. S2b), but only one contribution (Rt 2.9 min identified by an asterisk) peaks at 600 K.

MS/MS analyses were performed in both positive ($C_5H_{11}O_3^+$, m/z 119.0702) and negative ($C_5H_9O_3^-$, m/z 117.0556) modes. Fragmentation was conducted in an HCD cell (collision energy of 10 eV) generating several fragments. The study of these fragments was carried out in two steps. Firstly, the identification of the fragments that may derive from KHPs isomers (Supplementary Materials, Table S4) and secondly we plotted their profiles as a function of the JSR temperature. Only fragments with profiles peaking around 600 K were considered. MS/MS analyses using positive APCI, gave low-intensity fragments. Moreover, their profiles confirm co-elution of $C_5H_{10}O_3$ isomers other than KHPs. This can be explained by the presence of mass (m/z 119.0806) close that of the KHPs (m/z 119.0702) and which was collected by the Orbitrap despite the narrow mass window used (0.5 a.m.u) during targeted-SIM acquisitions. Besides higher ions signal intensity in negative APCI chromatograms (Fig. 10a), it was observed that the fragmentation of $C_5H_9O_3^-$ ions (negative APCI, m/z 117.0556) gives fragments (C_3H_5O , m/z 57.0346 and C_4H_7O m/z 71.0502) (Supplementary Materials, Table S4) having a profile similar to that expected for KHPs (Fig. 10b).

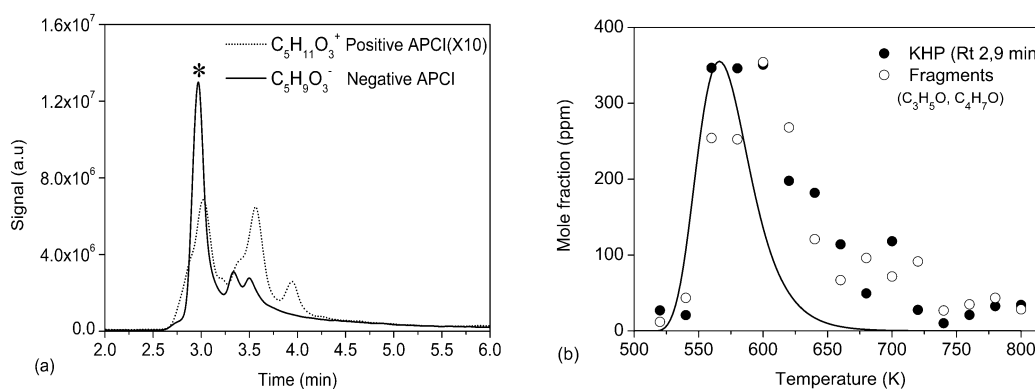


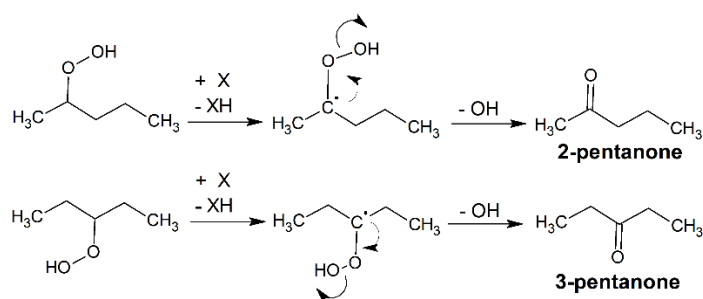
Fig. 10. (a) Chromatograms showing $C_5H_{11}O_3^+$ (m/z 119.0702) and $C_5H_9O_3^-$ (m/z 117.0556) corresponding to $C_5H_{10}O_3$ isomers obtained during the low temperature oxidation of n-pentane at 10 atm and 600 K. Silica Ascentis HPLC column was used. (b) Comparison between mole fraction profiles of KHPs: line: modeling, circle: KHP at Rt 2.9 min (*), open circle: sum of two fragments (C_3H_5O and C_4H_7O). Experimental data were obtained using a Silica Ascentis HPLC and APCI(-)-HRMS analyses; they were scaled to modeling. Experimental errors are estimated to be $\sim 40\%$.

4.4 Cyclic ethers and pentanones $C_5H_{10}O$

A wide range of cyclic ethers has been observed during fuels combustion [37, 38]. Decomposition and cyclization of hydroperoxyalkyl radicals form cyclic ethers and hydroxyl radicals: $\cdot\text{QOOH} \rightarrow \text{cyclic ether} + \cdot\text{OH}$ [39]. Nagata et al. [40] studied the formation pathway to 2-Methyltetrahydrofuran (2-Me-THF) during vapor-phase oxidation of pentane. They proposed that 2-Me-THF might be formed by addition of oxygen to 2-pentyl or 1-pentyl radicals.

UHPLC analyses, using a reversed phase C_{18} column and APCI (+/-)-HRMS, showed the presence of several chromatographic peaks corresponding to $\text{C}_5\text{H}_{10}\text{O}$ isomers (Fig. 11a). The analysis of a 2-Me-THF standard allowed identifying it at the retention time of 9.11 min. However, the non-availability of other standards, i.e., 1,2-epoxypentane, 2-ethyl-3-methyl oxirane, 2-ethyl oxetane, and 2,4 dimethyl oxetane, made it difficult to identify the other peaks (Rt 8.60, 9.36, and 10.32 min). The signal of 2-Me-THF obtained by HRMS was plotted and compared to GC data and modeling. We noticed that there is a strong similarity between the three profiles, the formation of 2-Me-THF goes through a maximum mole fraction at 760 K (Fig. 11b). Analysis of a pentanal standard indicates a retention time of 11.97 min (positive and negative ionization modes). No positive ion ($\text{C}_5\text{H}_{11}\text{O}^+$, m/z 87.0802) could be recorded in chromatographic analyses of the 720 K sample at this retention time (Fig. 11a). In negative ionization mode ($\text{C}_5\text{H}_9\text{O}^-$, m/z 85.0658) we observed presence of a peak at 11.97 min having a very weak signal corresponding to pentanal (Fig. 11a).

$\text{C}_5\text{H}_{10}\text{O}$ may also correspond to ketones (2-pentanone and 3-pentanone) which can result from reactions of ROOH (Scheme 2).



Scheme 2. Formation of 2- and 3-pentanone

Analysis of their standards allowed their identification in positive APCI chromatogram (Fig. 11a). One can see a co-elution at Rt 10.10 and 10.17 resulting from similar polarity of these isomers. Nevertheless, their two profiles could be plotted and compared to the recorded GC-FID signal (Fig. 12).

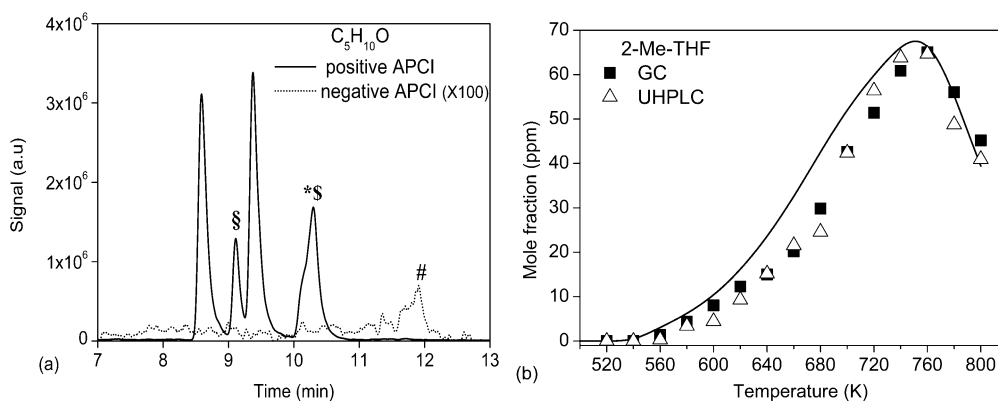


Fig. 11. (a) Chromatograms for $C_5H_{10}O$ obtained for a sample of n-pentane oxidation at 720 K, using a C_{18} UHPLC and APCI(+)-HRMS ($C_5H_{11}O^+$ at m/z 87.0802) and APCI(-)-HRMS ($C_5H_9O^-$ at m/z 85.0658). The APCI(-)-HRMS signal was multiplied by 100. §: (2-Me-THF), *: (2-pentanone), \$: 3-pentanone, and #: pentanal. (b) Comparison between 2-Me-THF mole fraction profiles obtained by GC-FID and UHPLC-APCI(+)-HRMS analyses with modeling data. UHPLC results were scaled to GC data.

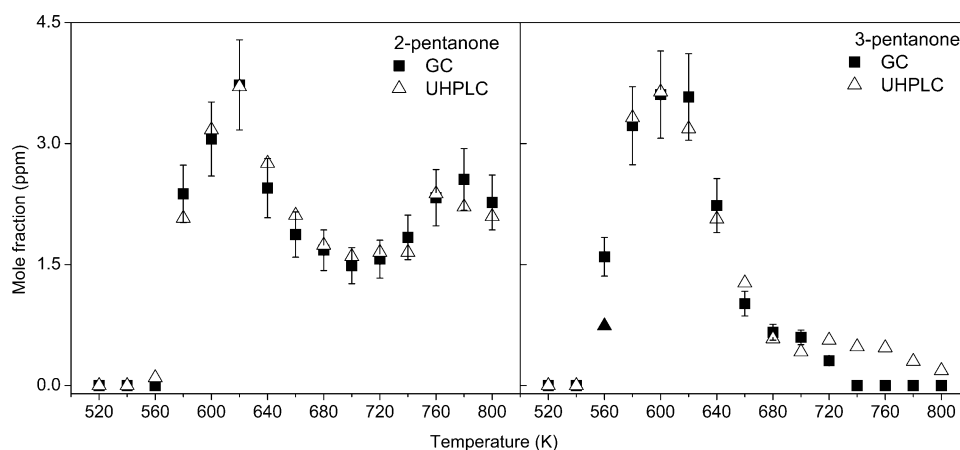
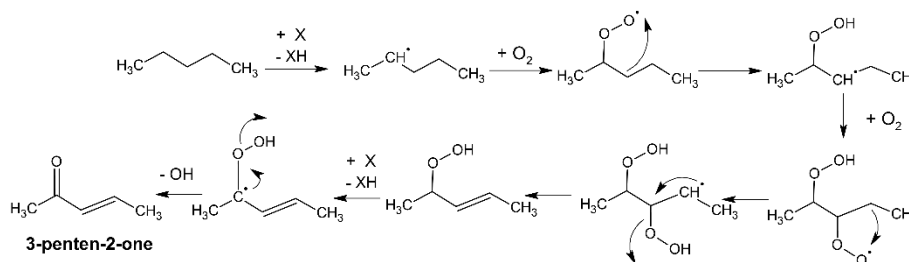


Fig. 12. Comparison between 2-pentanone and 3-pentanone mole fraction profiles obtained by C_{18} UHPLC APCI(+)-HRMS ($C_5H_{11}O^+$, m/z 87.0802) and GC analyses. UHPLC results were scaled to GC data. Results could not be compared with simulated profiles because these molecules are not present in the WS kinetic model.

4.5 Unsaturated ketones C_5H_8O

Unsaturated ketones (pentenones), like 3-penten-2-one can be formed during n-pentane low temperature oxidation after two O_2 additions on 2-pentyl radical and HO_2 elimination (Scheme 3).



Scheme 3. Formation of 3-penten-2-one

In addition to pentenones, C_5H_8O may correspond to other isomers such as cyclopentanone, 1-pentenal, 2-pentenal or cyclic ethers with one double bond (2,3-dihydropyran) resulting from the decomposition of $C_5H_{10}O$ species. The use of a C_{18} UHPLC column coupled to positive ($C_5H_9O^+$, m/z 85.0647) and negative ($C_5H_7O^-$, m/z 83.0501) APCI and HRMS revealed the presence of several chromatographic peaks (Supplementary Materials, Fig. S3). 3-Penten-2-one was identified at R_t 8.76 min. Its profile was plotted and compared to that obtained in GC analyses (Fig. 13). A cyclopentanone standard was analyzed (R_t 8.09 min) but no chromatographic peak was detected at this retention time (Supplementary Materials, Fig. S3). Unfortunately, 2,3-dihydropyran, 1-pentenal and 2-pentenal could not be identified by LC-HRMS analysis because of the unavailability of standards.

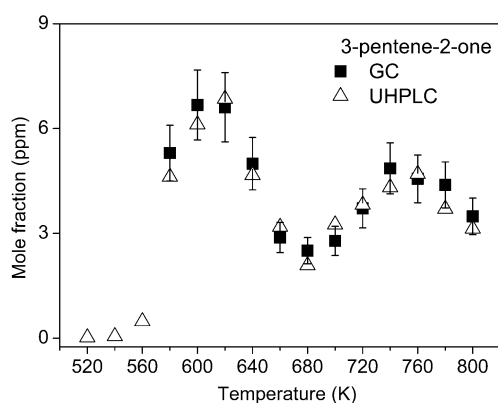
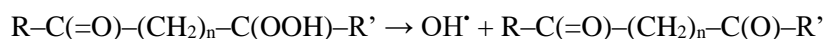


Fig. 13. Comparison of 3-pentene-2-one mole fraction profiles obtained after C_{18} UHPLC- APCI(+)-HRMS ($C_5H_9O^+$, m/z 85.0647) and GC-FID analyses. UHPLC data were scaled to those obtained in GC. Results could not be compared with computation profiles because these molecules are not present in the WS kinetic model.

4.6 Pentanediones $C_5H_8O_2$

Oxidation of n-alkanes can produce diones (diketones) through several pathways. Pelucchi et al. [41] proposed that heptanediones formed during low temperature oxidation of n-heptane, are directly produced by H-atom abstraction on KHPs by fuel radicals. Thus, for n-pentane, pentanediones can be formed as follows: $R^{\bullet} + C_5H_{10}O_3^{ij} \rightarrow RH + C_5H_8O_2^{ij} + OH^{\bullet}$. (i,j are the positions of carbonyl and hydroperoxy groups in KHPs). Ketohydroperoxides can undergo a roaming reaction to produce water and diones [42]. Blin-Simiand et al. [43] in their study of the oxidation of n-dodecane proposed that diones are products deriving from ketohydroperoxides decomposition:



Then, the sequence of reactions continues through isomerization:



Afterwards, the reaction proceeds via an addition of O_2 , itself followed by internal H-shift to form HO_2 and a diketone: $R-C(=O)-(CH_2)_n-C^*(OH)-R' + O_2 \rightarrow R-C(=O)-(CH_2)_n-C(OO^{\bullet})(OH)-R' \rightarrow R-C(=O)-(CH_2)_n-C(OOH)(O^{\bullet})-R' \rightarrow HO_2^{\bullet} + R-C(=O)-(CH_2)_n-C(=O)-R'$.

UHPLC- APCI(+)-HRMS analyses using a C_{18} column showed many peaks for $C_5H_8O_2$ ($C_5H_9O_2^+$, m/z 101.0593) (Supplementary Materials, Fig. S4). 2,4-Pentanedione (Rt 7.32 min) and 2,3-pentanedione (Rt 8.05 min) were identified using standards. Profiles as a function of reactor temperature were plotted and compared to GC mole fractions data (Fig. 14a and b). The results indicated that the production of 2,4-pentanedione is greater than that of 2,3-pentanedione (Supplementary Materials, Fig. S4). We also noticed that 2,4-pentanedione reaches a maximum at 600 K. However, 2,3-pentanedione peaks around 740 K. That might be explained by the fact these two diones are not formed by the same reaction pathways and do not come from the same precursors which are formed at different temperatures. $C_5H_8O_2$ also corresponds to other isomers like cyclic ether with a carbonyl group (2-methyltetrahydrofuran-3-one (2-Me-THF-3-one) known as coffee furanone, and tetrahydropyran-3-one), but we had no standards to identify them and confirm their formation under these experimental conditions (Table 1).

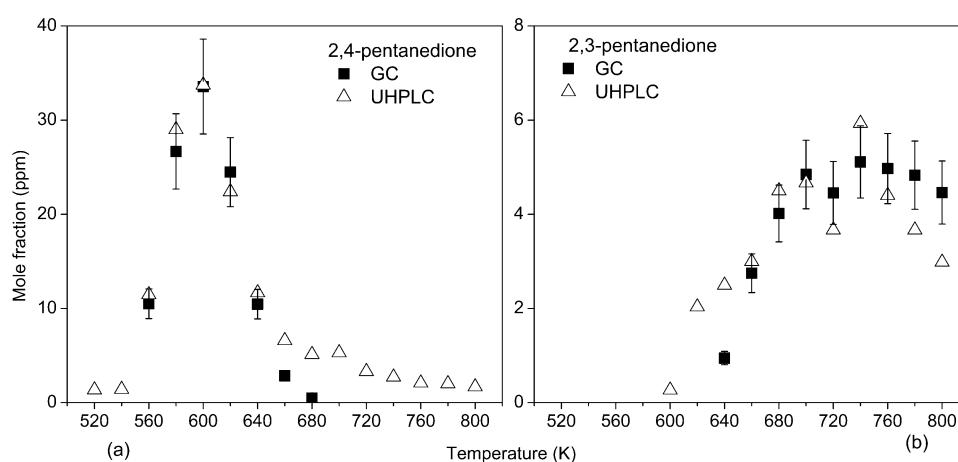


Fig. 14. Comparison between 2,4-pentanedione (a) and 2,3-pentanedione (b) mole fractions obtained by GC-FID and UHPLC- APCI(+)-HRMS ($C_5H_9O_2^+$, m/z 101.0593). UHPLC data were scaled to GC-FID data. Results could not be compared with simulations because these molecules are not included in the WS kinetic model.

4.7 Highly oxygenated molecules $C_5H_{12}O_4$, $C_5H_{10}O_4$, $C_5H_8O_4$, $C_5H_{10}O_5$, and $C_5H_{10}O_7$

More oxygenated molecules with one or more hydroperoxy groups are formed during n-pentane oxidation, as already reported in recent studies the oxidation of other fuels (alkanes, ethers)[17-22]. Thanks to the use of liquid phase sampling and high-resolution mass spectrometry, signals corresponding to highly oxygenated molecules including dihydroperoxides ($C_5H_{12}O_4$), unsaturated dihydroperoxides ($C_5H_{10}O_4$), and diketo-hydroperoxides ($C_5H_8O_4$) were detected using FIA and APCI(+/-)-HRMS (Table 2). We noticed that APCI(-) signal is greater than that obtained in positive mode, which implies that these HOMs are better ionized using negative APCI. Experimental results for $C_5H_{10}O_4$ and $C_5H_8O_4$ obtained by FIA-APCI(-)-HRMS ($C_5H_9O_4^-$, m/z 133.0506 and $C_5H_7O_4^-$, m/z 131.0350) were plotted and compared to their simulated profiles (Fig. 15a and c). One can see a difference of ~ 40 K between experimental and simulated peak of concentration for $C_5H_8O_4$ and $C_5H_{10}O_4$.

This temperature deviation was observed for other products as reported in previous paragraphs. Dihydroperoxides ($C_5H_{12}O_4$) were not considered in the WS model. Only FIA APCI(-)-HRMS results ($C_5H_{11}O_4^-$, m/z 135.0663) are presented in Fig. 15b. Signals corresponding to keto-dihydroperoxides ($C_5H_{10}O_5$), and keto-trihydroperoxides ($C_5H_{10}O_7$) formed through 3rd and 4th O_2 addition on fuel's radicals were detected only using FIA and negative APCI mode. H/D exchange confirmed the presence of OOH function in these species (Table 2). However, the instability and the weak signal did not allow acquiring ions signal profiles as a function of temperature.

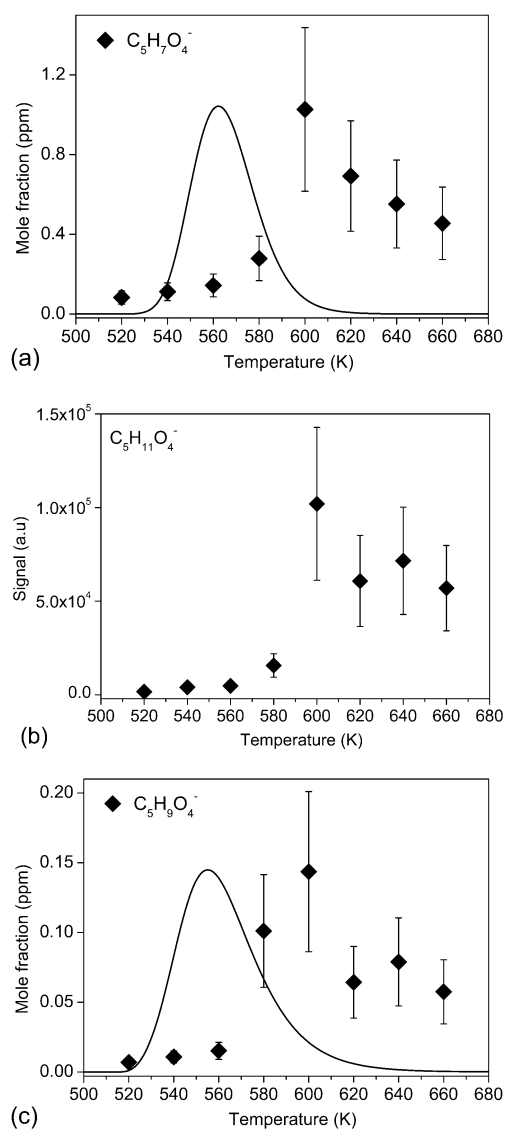


Fig. 15. Formation of HOMs $C_5H_8O_4$, $C_5H_{12}O_4$, and $C_5H_{10}O_4$ produced during the low temperature oxidation of n-pentane. Comparison between experimental results (symbols) using FIA APCI(-)-HRMS ($C_5H_7O_4^-$ at m/z 131.0350, $C_5H_{11}O_4^-$ at m/z 135.0663, and $C_5H_9O_4^-$ at m/z 133.0506) and modeling data (line) for $C_5H_{10}O_4$, and $C_5H_8O_4$. Experimental data were scaled to simulated results. HRMS errors are estimated to be $\sim 40\%$.

5. Conclusion and Perspectives

The low temperature (520-800 K) oxidation of 2500 ppm n-pentane was studied in a JSR at 10 atm and fuel-lean conditions. Besides GC and FTIR analyses providing new quantitative data, high resolution mass spectrometry coupled to liquid phase analysis methods (FIA, HPLC, and UHPLC) allowed the detection and separation of specific low temperature oxidation intermediates and products. Indeed, in addition to pentanediones, cyclic ethers, pentanones, pentenones, and other less explored molecules have been observed: C₃-C₅ alkylhydroperoxides, C₂-C₅ alkenylhydroperoxides, C₃-C₅ keto-hydroperoxides, and highly oxygenated molecules (C₅H₈O₄, C₅H₁₂O₄, C₅H₁₀O₄, C₅H₁₀O₅, C₅H₁₀O₇) resulting from the addition of up to 4 molecules of O₂ on pentyl radicals. We used H/D exchange with D₂O to confirm the presence of hydroxyl or hydroperoxyl groups in n-pentane oxidation products. Experimental results obtained for species considered in the WS kinetic model were compared to simulation results, showing some discrepancies (overestimation of the fuel's consumption below 600 K, overprediction of hydrogen, butanal, and formic acid mole fractions, underprediction of mole fractions of carbon dioxide in the cool flame and of methanol, ethanol, acetic acid, 2,5-dimethylfuran, 2- and 3-pentanone, pentanediones, 1,3-butadiene, and 1,3-pentadiene mole fractions). The present data for these species and for other cool flames specific products among which 15 are reported for the first time should be useful for improving existing chemical kinetic models. Formation pathways for under- and over-predicted products needs to be revisited. The present data should be helpful for that. The inclusion of formation routes to HOMs via multiple additions of O₂ and internal H-shifts would be needed to simulate their formation under combustion relevant conditions. Further investigations of n-pentane oxidation using different analytical techniques, e.g., molecular beam-mass spectrometry with synchrotron photoionization, other laboratory experiments, e.g., RCM or piston engines, and other operating conditions, e.g., different pressure, would be useful for further assessing the fuel's low temperature oxidation chemistry.

Acknowledgements

The authors gratefully acknowledge funding from the Labex Caprysses (convention ANR-11-LABX-0006-01) and from the Région Centre Val de Loire, EFRD, and CPER (projects PROMESTOCK and APROPOR-E).

References

- [1] S. Liu; Y. Okuyama; M. Tamura; Y. Nakagawa; A. Imai; K. Tomishige, Selective transformation of hemicellulose (xylan) into n-pentane, pentanols or xylitol over a rhenium-modified iridium catalyst combined with acids, *Green Chemistry* 18 (1) (2016) 165-175.
- [2] Z. Xinghua; W. Tiejun; M. Longlong; W. Chuangzhi, Aqueous-phase catalytic process for production of pentane from furfural over nickel-based catalysts, *Fuel* 89 (10) (2010) 2697-2702.
- [3] A. T. Navinprasad; R. Prakash; J. Yoganandh; B. Meenakshipriya; K. Ramakrishnan, Experimental Investigation of Nickel Oxide Nanomaterials with n-Pentane Diesel Blends in Compression Ignition Engine, *IOP Conference Series: Materials Science and Engineering* 1070 (2021) 012126.
- [4] M. Elkelawy; H. Alm-Eldin Bastawissi; E. A. El Shenawy; M. Taha; H. Panchal; K. K. Sadasivuni, Study of performance, combustion, and emissions parameters of DI-diesel engine fueled with algae biodiesel/diesel/n-pentane blends, *Energy Conversion and Management: X* 10 (2021) 100058.

- [5] H. Jin; J. Pieper; C. Hemken; E. Bräuer; L. Ruwe; K. Kohse-Höinghaus, Chemical interaction of dual-fuel mixtures in low-temperature oxidation, comparing n-pentane/dimethyl ether and n-pentane/ethanol, *Combust. Flame* 193 (2018) 36-53.
- [6] R. Hughes; R. F. Simmons, The low-temperature combustion of n-pentane, *Symposium (International) on Combustion* 12 (1) (1969) 449-461.
- [7] J. H. Knox; C. G. Kinnear, The mechanism of combustion of pentane in the gas phase between 250° and 400°C, *Symposium (International) on Combustion* 13 (1) (1971) 217-227.
- [8] J. Bugler; K. P. Somers; E. J. Silke; H. J. Curran, Revisiting the Kinetics and Thermodynamics of the Low-Temperature Oxidation Pathways of Alkanes: A Case Study of the Three Pentane Isomers, *J. Phys. Chem. A* 119 (28) (2015) 7510-7527.
- [9] J. Bugler; A. Rodriguez; O. Herbinet; F. Battin-Leclerc; C. Togbe; G. Dayma; P. Dagaut; H. J. Curran, An experimental and modelling study of n-pentane oxidation in two jet-stirred reactors: The importance of pressure-dependent kinetics and new reaction pathways, *Proc. Combust. Inst.* 36 (1) (2017) 441-448.
- [10] A. Rodriguez; O. Herbinet; Z. Wang; F. Qi; C. Fittschen; P. R. Westmoreland; F. Battin-Leclerc, Measuring hydroperoxide chain-branching agents during n-pentane low-temperature oxidation, *Proc. Combust. Inst.* 36 (1) (2017) 333-342.
- [11] J. Bourgalais; Z. Gouid; O. Herbinet; G. A. Garcia; P. Arnoux; Z. D. Wang; L. S. Tran; G. Vanhove; M. Hochlaf; L. Nahon; F. Battin-Leclerc, Isomer-sensitive characterization of low temperature oxidation reaction products by coupling a jet-stirred reactor to an electron/ion coincidence spectrometer: case of n-pentane, *Phys. Chem. Chem. Phys.* 22 (3) (2020) 1222-1241.
- [12] Z. D. Wang; B. J. Chen; K. Moshhammer; D. M. Popolan-Vaida; S. Sioud; V. S. B. Shankar; D. Vuilleumier; T. Tao; L. Ruwe; E. Brauer; N. Hansen; P. Dagaut; K. Kohse-Hoinghaus; M. A. Raji; S. M. Sarathy, n-Heptane cool flame chemistry: Unraveling intermediate species measured in a stirred reactor and motored engine, *Combust. Flame* 187 (2018) 199-216.
- [13] Z. Wang; D. M. Popolan-Vaida; B. Chen; K. Moshhammer; S. Y. Mohamed; H. Wang; S. Sioud; M. A. Raji; K. Kohse-Höinghaus; N. Hansen; P. Dagaut; S. R. Leone; S. M. Sarathy, Unraveling the structure and chemical mechanisms of highly oxygenated intermediates in oxidation of organic compounds, *Proceedings of the National Academy of Sciences* 114 (50) (2017) 13102-13107.
- [14] Z. Wang; S. Y. Mohamed; L. Zhang; K. Moshhammer; D. M. Popolan-Vaida; V. S. B. Shankar; A. Lucassen; L. Ruwe; N. Hansen; P. Dagaut; S. M. Sarathy, New insights into the low-temperature oxidation of 2-methylhexane, *Proc. Combust. Inst.* 36 (1) (2017) 373-382.
- [15] Z. D. Wang; S. M. Sarathy, Third O-2 addition reactions promote the low-temperature auto-ignition of n-alkanes, *Combust. Flame* 165 (2016) 364-372.
- [16] Z. Wang; L. Zhang; K. Moshhammer; D. M. Popolan-Vaida; V. S. B. Shankar; A. Lucassen; C. Hemken; C. A. Taatjes; S. R. Leone; K. Kohse-Hoeinghaus; N. Hansen; P. Dagaut; S. M. Sarathy, Additional chain-branching pathways in the low-temperature oxidation of branched alkanes, *Combust. Flame* 164 (2016) 386-396.
- [17] N. Belhadj; R. Benoit; P. Dagaut; M. Lailliau; Z. Serinyel; G. Dayma; F. Khaled; B. Moreau; F. Foucher, Oxidation of di-n-butyl ether: Experimental characterization of low-temperature products in JSR and RCM, *Combust. Flame* 222 (2020) 133-144.
- [18] N. Belhadj; R. Benoit; P. Dagaut; M. Lailliau, Experimental characterization of n-heptane low-temperature oxidation products including keto-hydroperoxides and highly oxygenated organic molecules (HOMs), *Combust. Flame* 224 (2021) 83-93.
- [19] N. Belhadj; R. Benoit; P. Dagaut; M. Lailliau, Experimental Characterization of Tetrahydrofuran Low-Temperature Oxidation Products Including Ketohydroperoxides and Highly Oxygenated Molecules, *Energy Fuels* 35 (9) (2021) 7242-7252.
- [20] N. Belhadj; R. Benoit; P. Dagaut; M. Lailliau; B. Moreau; F. Foucher, Low-temperature oxidation of a gasoline surrogate: Experimental investigation in JSR and RCM using high-resolution mass spectrometry, *Combust. Flame* 228 (2021) 128-141.
- [21] N. Belhadj; R. Benoit; P. Dagaut; M. Lailliau; Z. Serinyel; G. Dayma, Oxidation of di-n-propyl ether: Characterization of low-temperature products, *Proc. Combust. Inst.* 38 (1) (2021) 337-344.
- [22] N. Belhadj; R. Benoit; M. Lailliau; V. Glasziou; P. Dagaut, Oxidation of diethyl ether: Extensive characterization of products formed at low temperature using high resolution mass spectrometry, *Combust. Flame* 228 (2021) 340-350.
- [23] N. Belhadj; M. Lailliau; R. Benoit; P. Dagaut, Experimental and kinetic modeling study of n-hexane oxidation. Detection of complex low-temperature products using high-resolution mass spectrometry, *Combust. Flame* (2021) <https://doi.org/10.1016/j.combustflame.2021.111581>.
- [24] Z. Wang; M. Ehn; M. P. Rissanen; O. Garmash; L. Quelever; L. Xing; M. Monge-Palacios; P. Rantala; N. M. Donahue; T. Berndt; S. M. Sarathy, Efficient alkane oxidation under combustion engine and atmospheric conditions, *Communications Chemistry* 4 (1) (2021)

- [25] H. Tong; Y. Zhang; A. Filippi; T. Wang; C. Li; F. Liu; D. Leppla; I. Kourtchev; K. Wang; H.-M. Keskinen; J. T. Levula; A. M. Arangio; F. Shen; F. Ditas; S. T. Martin; P. Artaxo; R. H. M. Godoi; C. I. Yamamoto; R. A. F. de Souza; R.-J. Huang; T. Berkemeier; Y. Wang; H. Su; Y. Cheng; F. D. Pope; P. Fu; M. Yao; C. Pöhlker; T. Petäjä; M. Kulmala; M. O. Andreae; M. Shiraiwa; U. Pöschl; T. Hoffmann; M. Kalberer, Radical Formation by Fine Particulate Matter Associated with Highly Oxygenated Molecules, *Environmental Science & Technology* 53 (21) (2019) 12506-12518.
- [26] P. Roldin; M. Ehn; T. Kurtén; T. Olenius; M. P. Rissanen; N. Sarnela; J. Elm; P. Rantala; L. Hao; N. Hyttinen; L. Heikkinen; D. R. Worsnop; L. Pichelstorfer; C. Xavier; P. Clusius; E. Öström; T. Petäjä; M. Kulmala; H. Vehkamäki; A. Virtanen; I. Riipinen; M. Boy, The role of highly oxygenated organic molecules in the Boreal aerosol-cloud-climate system, *Nature Communications* 10 (1) (2019) 4370.
- [27] R. Benoit; N. Belhadj; M. Lailliau; P. Dagaut, On the similarities and differences between the products of oxidation of hydrocarbons under simulated atmospheric conditions and cool flames, *Atmos. Chem. Phys.* 21 (10) (2021) 7845-7862.
- [28] P. Dagaut; M. Cathonnet; J. P. Rouan; R. Foulatier; A. Quilgars; J. C. Boettner; F. Gaillard; H. James, A Jet-Stirred Reactor for Kinetic-Studies of Homogeneous Gas-Phase Reactions at Pressures up to 10-Atmospheres (~ 1 MPa), *Journal of Physics E-Scientific Instruments* 19 (3) (1986) 207-209.
- [29] P. Dagaut; M. Cathonnet; J. C. Boettner; F. Gaillard, Kinetic modeling of ethylene oxidation, *Combust. Flame* 71 (3) (1988) 295-312.
- [30] P. Dagaut; M. Cathonnet; J. C. Boettner; F. Gaillard, Kinetic Modeling of Propane Oxidation, *Combust. Sci. Technol.* 56 (1-3) (1987) 23-63.
- [31] A. El Bakali; P. Dagaut; L. Pillier; P. Desgroux; J. F. Pauwels; A. Rida; P. Meunier, Experimental and modeling study of the oxidation of natural gas in a premixed flame, shock tube, and jet-stirred reactor, *Combust. Flame* 137 (1-2) (2004) 109-128.
- [32] T. Le Cong; P. Dagaut, Experimental and Detailed Modeling Study of the Effect of Water Vapor on the Kinetics of Combustion of Hydrogen and Natural Gas, Impact on NO_x, *Energy Fuels* 23 (1) (2009) 725-734.
- [33] A. Ristori; P. Dagaut; M. Cathonnet, The oxidation of n-hexadecane: Experimental and detailed kinetic modeling, *Combust. Flame* 125 (3) (2001) 1128-1137.
- [34] P. Glarborg; R. J. Kee; J. F. Grcar; J. A. Miller in: *PSR: A FORTRAN program for modeling well-stirred reactors.*, SAND86-8209, Sandia National Laboratories, Livermore, CA, 1986
- [35] R. J. Kee; F. M. Rupley; J. A. Miller in: *CHEMKIN-II: A Fortran Chemical Kinetics Package for the Analysis of Gas-Phase Chemical Kinetics.*, SAND89-8009, Sandia National Laboratories, Livermore, CA, 1989
- [36] A. Jalan; I. M. Alecu; R. Meana-Paneda; J. Aguilera-Iparraguirre; K. R. Yang; S. S. Merchant; D. G. Truhlar; W. H. Green, New Pathways for Formation of Acids and Carbonyl Products in Low-Temperature Oxidation: The Korcek Decomposition of gamma-Ketohydroperoxides, *J. Am. Chem. Soc.* 135 (30) (2013) 11100-11114.
- [37] P. Dagaut; M. Reuillon; M. Cathonnet; D. Presvots, Gas-Chromatography and Mass-Spectrometry Identification of Cyclic Ethers Formed from Reference Fuels Combustion, *Chromatographia* 40 (3-4) (1995) 147-154.
- [38] O. Herbinet; S. Bax; P.-A. Glaude; V. Carre; F. Battin-Leclerc, Mass spectra of cyclic ethers formed in the low-temperature oxidation of a series of n-alkanes, *Fuel* 90 (2) (2011) 528-535.
- [39] F. Buda; R. Bounaceur; V. Warth; P. A. Glaude; R. Fournet; F. Battin-Leclerc, Progress toward a unified detailed kinetic model for the autoignition of alkanes from C₄ to C₁₀ between 600 and 1200 K, *Combust. Flame* 142 (1-2) (2005) 170-186.
- [40] H. Nagata; Y. Takiyama; M. Kishida; K. Wakabayashi; N. Yamamoto, Pathway of the Formation of 2-Methyltetrahydrofuran from Pentane in Vapor-phase Oxidation, *J. Jpn. Pet. Inst.* 38 (3) (1995) 203-207.
- [41] M. Pelucchi; M. Bissoli; C. Cavallotti; A. Cuoci; T. Faravelli; A. Frassoldati; E. Ranzi; A. Stagni, Improved Kinetic Model of the Low-Temperature Oxidation of n-Heptane, *Energy Fuels* 28 (11) (2014) 7178-7193.
- [42] R. H. West; C. F. Goldsmith, The impact of roaming radicals on the combustion properties of transportation fuels, *Combust. Flame* 194 (2018) 387-395.
- [43] N. Blin-Simiand; F. Jorand; K. Sahetchian; M. Brun; L. Kerhoas; C. Malosse; J. Einhorn, Hydroperoxides with zero, one, two or more carbonyl groups formed during the oxidation of n-dodecane, *Combust. Flame* 126 (1) (2001) 1524-1532.